AIAA SciTech Forum
8-12 January 2024, Orlando, FL
AIAA SCITECH 2024 Forum

10.2514/6.2024-0691

In-Situ Diagnostic of Channel Erosion in Hall Thrusters

Ivan Romadanov[1]
Princeton Plasma Physics Laboratory, Princeton, NJ 08543, USA

Ishaan Mishra[2]
Rose-Hulman Institute of Technology, Terre Haute, Indiana, 47803, USA

Jacob Kiviat[3]
Cornell University, Ithaca, NY, 14853, USA

Sung Hyun Son[4]
Princeton University, Princeton, NJ 08543, USA

Benjamin Benjadol[5]
Princeton University, Princeton, NJ 08543, USA

Angelica Ottaviano[6]

UCLA, Los Angeles, California 90095, USA

Michael Keidar[7]
George Washington University, Washington, DC 20052, United States of America

Yevgeny Raitses[8]
Princeton Plasma Physics Laboratory, Princeton, NJ 08543, USA

In this work, we introduce a design of a high-resolution optical diagnostic system for in situ monitoring and measurements of wall erosion in electric propulsion devices. Focused on addressing erosion in Hall thrusters, we explore a recently proposed strategy of the accelerated erosion test which exploits the angular dependence of the ion-induced sputtering yield to enhance erosion of micropatterned channel walls. The developed erosion diagnostic incorporates a Long-Distance Microscope (LDM), positioned outside the vacuum chamber to simplify operation. It achieves a narrow in-focus range over distances greater than 1 meter,

[1] Associate research physicist, Applied Materials and Sustainability Sciences.
[2] Undergraduate, Physics and Optical Engineering, and AIAA University Student Member.
[3] Undergraduate, Applied and Engineering Physics.
[4] Graduate Student, Department of Astrophysical Sciences.
[5] Undergraduate, Mechanical and Aerospace Engineering, AIAA university student member.
[6] Research Engineer, Mechanical and Aerospace Engineering Dept.
[7] Professor, Mechanical and Aerospace Engineering, AIAA fellow.
[8] Principal Research Physicist, Discovery Plasma Science, associate AIAA fellow

enabling the use of a shape-from-focus algorithm for 3D object geometry reconstruction with resolutions in the tens of micrometers. Initial tests utilized a boron nitride target with wall pattern optimized for maximum erosion rates. The target was exposed a 600 eV ion beam generated by a gridded ion source. The LDM setup was validated by comparing measurements of the uneroded target with the 3D computer design model data. In this initial test, a resolution of about $70\mu m$ was achieved.

I. Nomenclature

BCA	=	Binary Collision Approximation
SFF	=	shape from focus
BN	=	boron nitride
DOF	=	depth of focus
LDM	=	Long-Distance Microscope
WD	=	Working Distance
L	=	LDM range of motion
λ	=	wavelength
n	=	index of refraction
NA	=	numerical aperture
Y_n	=	sputter yield at normal angle of incidence
θ	=	ion incidence angle

II. Introduction

Electric Propulsion (EP) systems, crucial for high-power in-space applications, face challenges in accurately predicting performance and lifetime, vital for advancing space missions. Efforts to extend satellite on-orbit service times, including re-fueling[1] and increasing thruster power[2,3], present new challenges for ground testing facilities in enhancing lifetime prediction accuracy and formulating new testing strategies. Accelerated testing, aiming to predict thruster lifetime within shorter durations and offering cost and time efficiencies, requires developing predictive models to understand plasma interactions with thruster channel walls and electrodes, leading to material removal through sputtering, etching, and desorption.

Despite advancements in plasma-wall interaction models and material databases, predictive capabilities for plasma propulsion are limited[4,5]. Effective predictive modeling for thruster lifetime relies on a reliable validation method, traditionally involving lengthy and expensive thruster operation[6–9]. An alternative to this costly and time-consuming method is accelerated testing under elevated operational conditions like higher power settings. Yet, this approach's viability for model validation and lifetime prediction depends on whether these conditions alter the physical mechanisms responsible for thruster aging. Thus, identifying key failure mechanisms and developing physical models and scaling laws for these conditions is essential. In Hall thrusters, erosion of thruster channel walls, primarily due to ion-induced sputtering of materials like BN ceramic[10–13], significantly impacts lifetime. The sputtering yield depends on the mass, energy of the impinging ions, their angle of incidence, particle flux, and exposure duration, all crucial in determining the erosion rate[14].

For accelerated testing to accurately predict Hall thruster lifetime under realistic conditions, it must replicate specific erosion processes, including the chemical and physical changes in channel wall materials. This includes complex chemical changes in advanced boron nitride ceramics used in Hall thrusters (e.g., grades M2 and M26), involving boron nitride depletion and stress-induced micro-cracking[11,15].

To preserve essential erosion mechanisms, particularly sputtering, we would like to explore a strategy where thrusters operate under normal conditions but with materials designed for enhanced wear. This method uses test channel wall materials, identical in chemical composition and structure to standard boron nitride ceramic, with machined grooves near the exit to optimize sputtering yield and control erosion rate acceleration. These grooves, based on the principle that sputtering yield $\sim(\cos\theta)^{-1}$[14,24], where θ the ion incidence angle, are engineered to enhance erosion rates. For instance, preliminary estimations with monoenergetic Argon ions show that at a 75-degree incidence angle, erosion occurs about four times faster than at an average angle of 30-40 degrees.

Accurate, in-situ erosion monitoring is critical for optimizing processes and understanding the physics involved. Existing diagnostic methods, including in-situ laser holography[16] and microscopy[17–19], have limitations like limited resolution and complex setup requirements. In electric propulsion, techniques such as mass change control[20], optical emission spectroscopy[21], mass spectrometry[22], laser spectroscopy[23,24], and telemicroscopy[25] have

been explored. However, only telemicroscopy directly measures erosion by tracking surface morphology changes. This research employs the LDM accompanied with the SFF algorithm to provide a simpler, external solution with high-resolution capabilities. The primary goal is to develop an in-situ diagnostic tool for real-time erosion assessment, suitable for electric propulsion and potentially other plasma devices. This tool, combining LDM and SFF[26–28], ensures high-resolution erosion monitoring. Initial tests used a Boron BN target, designed to enhance erosion rates, and a 3 cm Kaufman-type gridded ion source producing a 600 eV neutralized Argon ion beam. The reported detection limit of approximately 70μm , requires about 14 hours of operational time, shortening testing duration while replicating realistic erosion patterns.

This paper is structured as follows: Section III details the design of the BN target, the diagnostic tool, and the data collection and processing algorithm. Section IV outlines the experimental setup. Section V presents the results and accompanying discussion. Finally, Section VI concludes the paper.

III. Methodology

This section provides the overview of the methodology of this study, detailing the design of accelerated erosion tests, the development of the diagnostic tool, and outlines data collection and processing techniques.

A. Design of Accelerated Erosion Tests

An accelerated life test is designed to expedite erosion studies in Hall thruster channel walls, focusing specifically on areas of highest wear and the impact of operational parameters. To accelerate the erosion process, the ion incidence angle from the plasma onto the channel walls is optimized. This involves introducing grooves on the ceramic channel walls, shaped like right triangles with the hypotenuse facing the anode, as depicted in Fig. 1. These grooves, approximately 1-2 mm in size and located near the channel exit, cover ionization and acceleration regions where erosion rates are highest[11,29]. The expected increase in erosion on the wall facing the anode is due to the $\sim(\cos\theta)^{-1}$ dependency of erosion yield[14] on the angle of incidence. By varying the angles of the grooves on both the outer and inner channel walls, the erosion rate can be controlled.

For the tests described in this paper, a BN target was used to represent a simplified geometry and material of Hall thruster walls. The target, featuring grooves designed to maximize erosion rates, was developed based on theoretical modeling and binary collision simulations. Detailed descriptions of the target design, simulations, and modeling will be provided in subsequent sections.

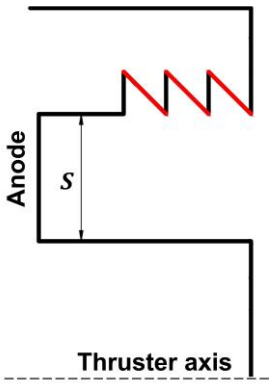

Fig. 1 Schematic of the proposed ceramic wall modification (not to scale, inner wall grooves are not shown). Surfaces marked with red will have the maximum erosion rate.

B. Diagnostic Tool

To ensure uninterrupted accelerated life tests, an LDM, combined with the SFF image processing algorithm, is utilized for real-time, in-situ monitoring of surface erosion and material deposition[26]. The SFF method continuously adjusts focus, capturing a sequence of images at different focal planes as the LDM translates towards the object in fixed steps. Each image in this sequence has different in-focus areas of the object, with some parts appearing well-focused and others blurred. The depth map is created by identifying the LDM position at which the focus measure for each pixel or region is maximized, resulting in a high-resolution topography map (a 2D matrix with elements indicating the LDM positions where corresponding pixels were most in-focus). This enables precise measurements of surface features and microstructures. The resolution of LDM systems, influenced by optical quality and camera sensor

type, can theoretically reach as low as a single μm, limited by the system's diffraction limit. The resolution is significantly affected by calculated as

$$\mathrm{DOF} = \frac{\lambda\sqrt{n^2 - NA^2}}{NA^2} \tag{1}$$

To optimize this, the light source with a blue light was used to illuminate the target.

LDMs have been utilized alongside high-speed cameras for imaging electrospray thruster emissions[19]. Additionally, in-situ thermal characterization of ion thruster grids using a pyrometer has been demonstrated[17], where LDMs or telemicroscopes image grid holes to measure their sizes. LDM imaging has also been employed to qualitatively validate erosion values derived from Triangular Laser Head measurements[25]. In Sitael's Advanced Electric Propulsion Diagnostic system[18], an LDM combined with a laser system illuminates the surface with a narrow band of light. This setup enables the measurement of erosion-induced changes in surface structure, as observed through images captured by the LDM.

The PPPL optical platform for in-situ erosion measurements is engineered to provide vibration protection and high reliability. It features a modified LDM setup, based on the designs by Ottaviano et al.[26], with the optical system and image collection moved outside of the vacuum chamber while preserving resolution. This setup includes a Questar QM 1 MK III LDM, a Maksutov Cassegrain Catadioptric microscope capable of working distances up to 1.6 m, achieving a depth of focus (DOF) of 950 μm. A Velmex motorized stage offers precise control with a 6-inch range and a step size of 1.6 μm, maintaining a movement speed up to 1.5 mm per second. Vibration isolation is ensured by mounting the assembly on a specialized platform. Imaging is done with an Allied Vision Alvium 1800 U-500c camera, featuring a 5.0 MP sensor. The target is imaged through a mirror system via a viewport in the vacuum chamber, as depicted in Fig. 2.

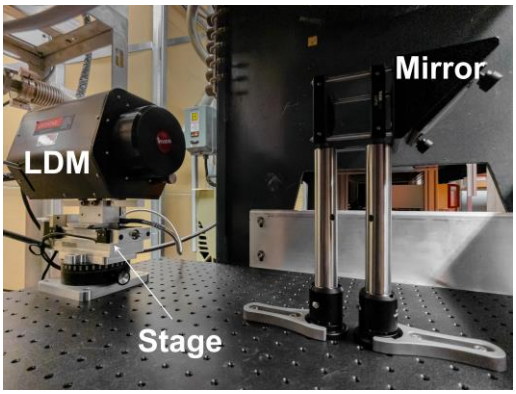

Fig. 2 LDM optical setup with the Velmex stage. Camera is not shown.

C. Data Collection and Processing

The SFF algorithm by Nayar et al.[27] generates surface depth maps using images from an LDM, which incrementally moves towards the target. Each step focuses on different parts of the object. The setup includes a semi-automated focus finder that accurately determines the starting position, defined when the target's central region is in focus. This algorithm calculates the focus measure at the target's center as a function of the LDM position and fits it with a Gaussian distribution to define the optimal focus. Scanning covers a range of 4-6 mm around the optimal focus position, with 20 μm steps. The Thorlabs M450LP2 collimated LED light, emitting at 450±18 nm, serves as the light source for imaging, utilizing shorter wavelengths for enhanced clarity. An unprocessed image sample at a specific LDM position is shown in Fig. 3.

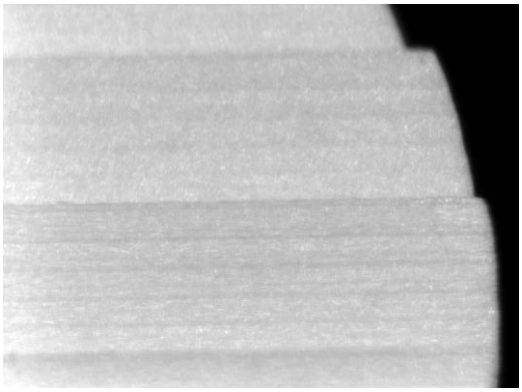

Fig. 3. Example of target image collected by LDM without post-processing.

The post-processing procedure includes initial image loading, noise reduction through smoothing, and alignment of images to their optical center. Due to challenges in achieving micrometer-precision alignment, images are aligned with the central pixel of the first image in the stack. Speckle noise is reduced using a median kernel filter. Focus-variation algorithms are then utilized to generate composite images, ensuring each pixel is in focus and measuring their relative depth. After testing several algorithms, algorithm described in Ref.[26] was found to yield the best results. In-focus pixels from each image are amalgamated into a single composite image for each stack. This leads to the creation of a high-resolution topography map by maximizing the focus measure for each pixel at the optimal LDM position. Several key updates were implemented in the algorithm to enhance performance. Parallel computing was utilized to increase processing speed by approximately five times. To address varying light conditions during experiments, each image's grayscale was adjusted to match the first image using MATLAB's "imhistmatch" function. The images were aligned to the first in the series using MATLAB functions, facilitating the creation of more accurate height map. This process uses a slightly modified algorithm by Ottaviano et al., detailed in Fig. 4.

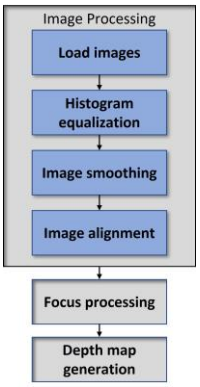

Fig. 4. Image processing algorithm.

IV. Experimental setup

Design of the BN target and description of experimental setup along with the data collection system are presented in this section.

A. Design of boron nitride target with maximized sputter yield

For the experiments described in this report, a h-BN ceramic target was designed to maximize the erosion rate and to allow for distinguishable surface changes during plasma operation. BCA simulations,[30] a subset of ion-material interaction software, were employed to inform the target design. Specifically, TRIM, a well-established BCA software, was used to study the angular dependence of incident ions on sputter yield. In TRIM, target atoms are distributed randomly based on target density, categorizing it as a Monte Carlo BCA software. The objective was to determine the optimal angle of incidence for maximized sputter yield. The optimal angle for maximum sputter yield was identified by fitting Yamamura's semi-empirical model[31] to TRIM simulations and experimental data from Chen et al. This simplified model is described as

$$Y_\theta = Y_n \cos^{-F}(\theta) e^G \quad (2)$$

Experimental data were gathered using 810 eV Argon ions on h-BN[32], and the model was verified for this dataset. To align the experimental results with TRIM simulations, the data at 810 eV were linearly scaled to 600 eV . This adjustment was made based on the observed linear dependence of incident ion energy on sputter yield within this energy range. The fitting process addresses the complexity of predicting sputtering in BN due to its regular crystal structure and varying values for parameters like surface binding energy. The results are presented in Fig. 5 for experimental data and TRIM simulations, respectively.

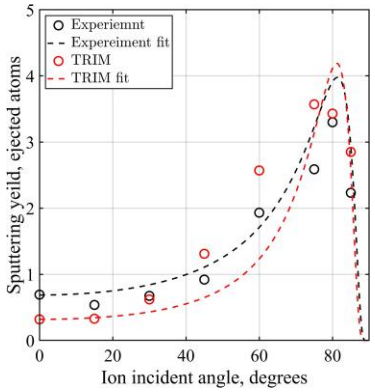

Fig. 5 Sputter yield as a function of ion incident angle for experimental and TRIM simulation data.

Based on these estimations, a target was designed such that the angle of incidence of an ion beam with the surface is 75°. Target design and its photo are presented in Fig. 6.

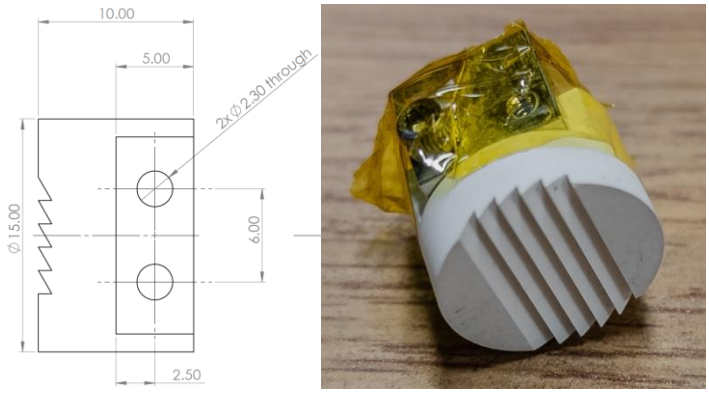

Fig. 6 Drawing (dimensions are in mm) and photo of the designed targed for accelerated erosion tests.

B. Vacuum facility and general setup overview

General schematic of the experimental setup is shown in Fig. 7. The Small Hall Thruster Facility (SHTF)[33] consist of a vacuum vessel equipped with a gas supply and power supplies. Vacuum vessel is a stainless-steel chamber measuring 1 m in length and 0.8 m in diameter. A combination of a blower, a mechanical pump, and an Osaka TG3203M turbo-molecular pumping system allows for achieving a base vacuum pressure of approximately $6 \cdot 10^{-6}\ Torr$. During operation, argon gas flow is controlled via a mass flow controller, adjustable from 0 to 10 sccm. Under these flow conditions, the background gas pressure, corrected for argon, remains below $6 \cdot 10^{-5}\ Torr$. Pressure measurements are conducted using an external ion gauge, which is mounted atop the vacuum chamber.

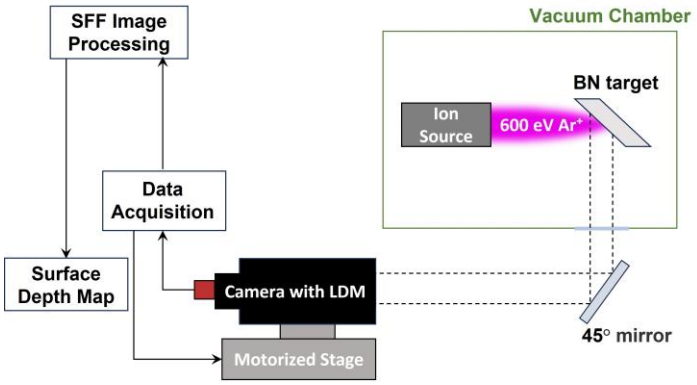

Fig. 7 General schematic of the experimental setup.

A 3-cm Kaufman-type gridded ion source is utilized to generate an Argon plasma and accelerate the Ar+ ions over a 600 V potential difference within the SHTF. The tungsten filament neutralizer, integrated into the ion source for emitting electrons to neutralize the ion beam, also serves as the light source for the h-BN target. The operating ion source and BN target are depicted in Fig. 8. Ion beam current at the target position was measured with specifically designed planar probe of 1.8 cm^2 area and at 5 sccm current density was 0.6 mA/cm^2.

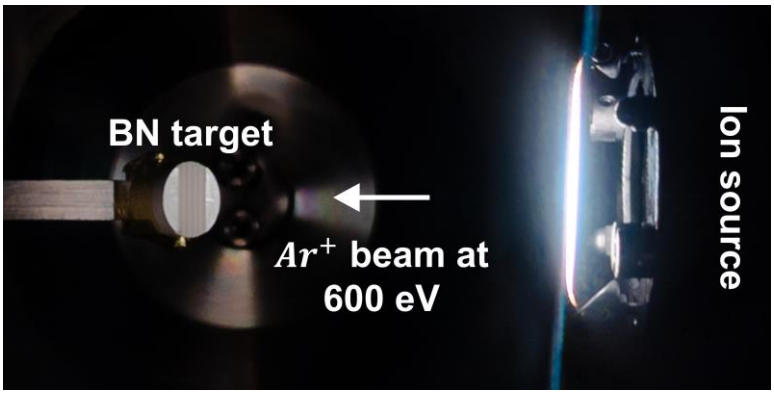

Fig. 8 Ion Source and BN target during operating

C. Data acquisition

Data acquisition and motion control are achieved through a combined use of a Raspberry Pi 4B and a RedPitaya STEMLab 125-14 and a motor controller. The code responsible for motor movement, image acquisition, and encoder signal collection is consolidated within a single program on the Raspberry Pi. This program records the distance traveled during each motor movement, allowing for subsequent comparison with depth map data generated using the SFF algorithm. The RedPitaya serves as a Data Acquisition System (DAQ) for encoder signals and as a triggering source for the motor controller. The operating code runs on the Raspberry Pi, which is also connected to the camera utilized for surface image acquisition. The overall flow of the operating code can be seen in the Fig. 6. After setting the acquisition conditions, the linear stage is centered, and image scanning is executed from x = -L/2 to x = L/2, based on the specified step size.

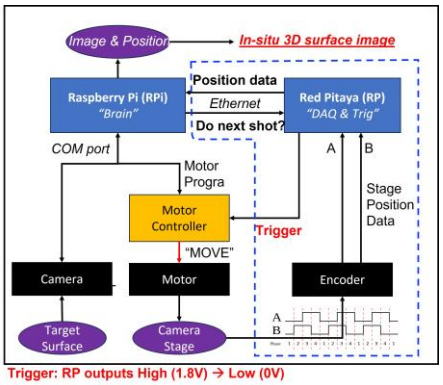

Fig. 9 Flow chart of the system for LDM operations.

V. Results and discussion

Measurements before target exposure to the ion beam are presented in Fig. 10. The SFF algorithm-generated heightmap is depicted in Fig. 10a. This reconstructed surface was averaged along the X-axis, and the resulting profile was compared with one from a 3D CAD model of the target surface. Both profiles, aligned for overlap, demonstrate close resemblance, although end regions were trimmed to avoid errors from optics vignetting. The difference between the measured and CAD profiles was quantified by taking a mean and standard deviation of their difference, yielding $\delta_{before} = 74 \pm 78\ \mu m$, which is exceeding the $20\ \mu m$ distance between images and previously reported[26]. The causes of this disparity are discussed later.

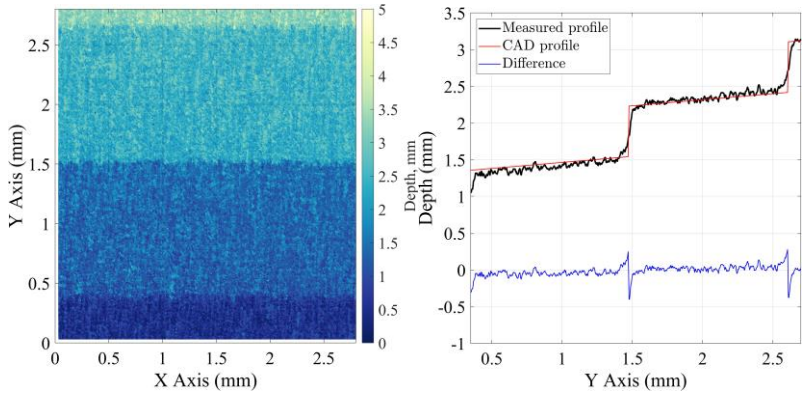

Fig. 10 Depth map obtained with SFF. Depth map profiles: SFF algorithm(black), CAD model (red) and their difference

After ion beam exposure measurements (~1.5 hours) are illustrated in Fig. 11. The post-exposure profile appears noisier, with a difference of $\delta_{after} = 95 \pm 120\ \mu m$ relative to the CAD profile. While there is a difference between δ_{before} and δ_{after}, this difference is much smaller than the errorbars. Estimations of the erosion over this exposure time are about 7 μm, which is smaller than the observed difference.

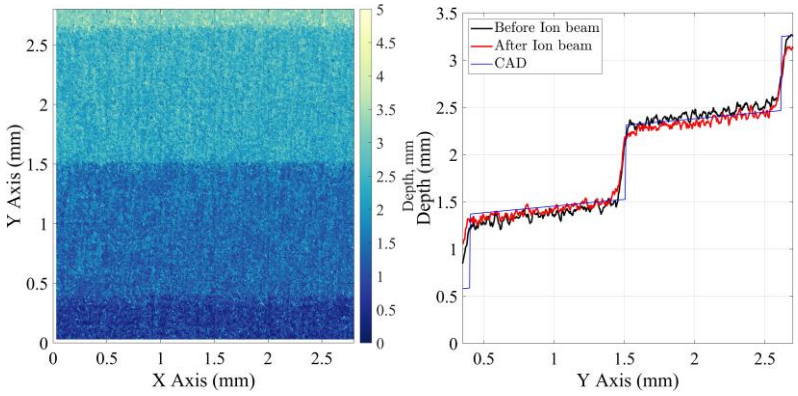

Fig. 11 Depth map obtained with SFF after 1 hour exposure. Depth map profiles: before the exposure (black), after the exposure (red) and CAD profile (blue)

Obtained error margins account for reconstruction errors and machining precision in the target profile. For instance, horizontal lines visible in Fig. 3, attributed to the cutting instrument, introduce noise into the recovered profile. Factors affecting image quality include image alignment imperfections, edge regions blur due to vignetting, variable illumination, and the need for algorithm optimization. Imperfect linear camera motion, due to motorized stage limitations, necessitates image alignment. Adjusting the angle between the main optical axis and light source could improve illumination. Further algorithm evaluation is needed, focusing on parameters like pixel sharpness estimation area, smoothing effects, focus measure definitions, number of images in a stack, and step size between them. By optimizing these factors, resolution of the system can be further improved.

VI. Conclusion

Addressing the challenge of lifetime and wear tests in Hall thrusters, this study explores a recently proposed strategy of the accelerated erosion test which exploits the angular dependence of the ion-induced sputtering yield to enhance erosion of micropatterned channel walls. The ability for in situ monitoring of the wall erosion is a critical requirement for the accelerated test. For that purpose, we developed and tested the Long-Distance Microscope (LDM) system placed outside the vacuum chamber. Combined with a shape-from-focus algorithm, the LDM system achieved $74 \pm 78\ \mu m$ resolution in 3D geometry reconstruction at a distance of about 1 m. Initial erosion tests with a 600 eV neutralized Ar ion beam generated by a gridded ion source showed the ability of the LDM to detect variations in erosion profiles compared to unexposed targets, showing correlation with theoretical erosion estimations. Further steps will involve the improvements of the measurement resolution and the adaptation of the LDM system for experiments with a 2 kW Hall thruster operated with Xe, Kr, N2 and air propellants[34].

Acknowledgments

Authors would like to thank Tim Bennett and Alex Merzhevsky for their help with technical setup and Adam Collins for helpful discussion. This work was supported by the Air Force Office of Scientific Research.

References

[1] Vaidya, S., Traub, C., Romano, F., Herdrich, G. H., Chan, Y.-A., Fasoulas, S., Roberts, P. C. E., Crisp, N. H., Edmondson, S., Haigh, S. J., Holmes, B. E. A., Macario-Rojas, A., Oiko, V. T. A., Smith, K. L., Sinpetru, L. A., Becedas, J., Sulliotti-Linner, V., Christensen, S., Hanessian, V., Jensen, T. K., Nielsen, J., Bisgaard, M., Garcia-Almiñana, D., Rodriguez-Donaire, S., Suerda, M., Garcia-Berenguer, M., Kataria, D., Villain, R., Seminari, S., Conte, A., and Belkouchi, B., "Development and Analysis of Novel Mission Scenarios Based on Atmosphere-Breathing Electric Propulsion (ABEP)," *CEAS Space Journal*, Vol. 14, No. 4, 2022, pp. 689–706. https://doi.org/10.1007/s12567-022-00436-1

[2] Kieckhafer, A., and King, L. B., "Energetics of Propellant Options for High-Power Hall Thrusters," *Journal of Propulsion and Power*, Vol. 23, No. 1, 2007, pp. 21–26. https://doi.org/10.2514/1.16376

[3] Peterson, P., Jacobson, D., Manzella, D., and John, J., "The Performance and Wear Characterization of a High-Power High-Isp NASA Hall Thruster," presented at the 41st AIAA/ASME/SAE/ASEE Joint Propulsion Conference & Exhibit, Tucson, Arizona, 2005. https://doi.org/10.2514/6.2005-4243

[4] Garrigues, L., Boniface, C., Hagelaar, G. J. M., Boeuf, J. P., and Duchemin, O., "Performance Modeling of a Thrust Vectoring Device for Hall Effect Thrusters," *Journal of Propulsion and Power*, Vol. 25, No. 5, 2009, pp. 1003–1012. https://doi.org/10.2514/1.39680

[5] Shagaida, A. A., Gorshkov, O. A., and Tomilin, D. A., "Influence of the Erosion of the Discharge Channel Wall on the Efficiency of a Stationary Plasma Thruster," *Technical Physics*, Vol. 57, No. 8, 2012, pp. 1083–1089. https://doi.org/10.1134/S1063784212080221

[6] Frieman, J. D., Kamhawi, H., Peterson, P. Y., Herman, D. A., Gilland, J. H., and Hofer, R. R., "Completion of the Long Duration Wear Test of the NASA HERMeS Hall Thruster," *AIAA Propulsion and Energy 2019 Forum*, American Institute of Aeronautics and Astronautics, 2019. https://doi.org/10.2514/6.2019-3895

[7] de Grys, K., Mathers, A., Welander, B., and Khayms, V., "Demonstration of 10,400 Hours of Operation on 4.5 kW Qualification Model Hall Thruster," *46th AIAA/ASME/SAE/ASEE Joint Propulsion Conference & Exhibit*, American Institute of Aeronautics and Astronautics, 2010. https://doi.org/10.2514/6.2010-6698

[8] Noord, J. V., "Lifetime Assessment of the NEXT Ion Thruster," *43rd AIAA/ASME/SAE/ASEE Joint Propulsion Conference & Exhibit*, American Institute of Aeronautics and Astronautics. https://doi.org/10.2514/6.2007-5274

[9] Fisher, J., "NEXT-C Flight Ion System Status," *AIAA Propulsion and Energy 2020 Forum*, American Institute of Aeronautics and Astronautics, 2020. https://doi.org/10.2514/6.2020-3604

[10] Tahara, H., Imanaka, K., and Yuge, S., "Effects of Channel Wall Material on Thrust Performance and Plasma Characteristics of Hall-Effect Thrusters," *Vacuum*, Vol. 80, No. 11, 2006, pp. 1216–1222. https://doi.org/10.1016/j.vacuum.2006.01.049

[11] Burton, T., Schinder, A. M., Capuano, G., Rimoli, J. J., Walker, M. L. R., and Thompson, G. B., "Plasma-Induced Erosion on Ceramic Wall Structures in Hall-Effect Thrusters," *Journal of Propulsion and Power*, Vol. 30, No. 3, 2014, pp. 690–695. https://doi.org/10.2514/1.B34882

[12] Yim, J., Boyd, I., and Keidar, M., "Hall Thruster Erosion Prediction Using A Hydrodynamic Plasma Model And Sputtering Simulation," 2007.

[13] Jin, C., Ottaviano, A., and Raitses, Y., "Secondary Electron Emission Yield from High Aspect Ratio Carbon Velvet Surfaces," *Journal of Applied Physics*, Vol. 122, No. 17, 2017, p. 173301. https://doi.org/10.1063/1.4993979

[14] Murty, M. V. R., "Sputtering: The Material Erosion Tool," *Surface Science*, Vol. 500, Nos. 1–3, 2002, pp. 523–544. https://doi.org/10.1016/S0039-6028(01)01586-2

[15] Brown, N. P., and Walker, M. L. R., "Review of Plasma-Induced Hall Thruster Erosion," *Applied Sciences*, Vol. 10, No. 11, 2020, p. 3775. https://doi.org/10.3390/app10113775

[16] Thomas, C. E. (Tommy), Granstedt, E. M., Biewer, T. M., Baylor, L. R., Combs, S. K., Meitner, S. J., Hillis, D. L., Majeski, R., and Kaita, R., "Digital Holography for *in Situ* Real-Time Measurement of Plasma-Facing-Component Erosion," *Review of Scientific Instruments*, Vol. 85, No. 11, 2014, p. 11D810. https://doi.org/10.1063/1.4886435

[17] Bundesmann, C., Tartz, M., Scholze, F., Neumann, H., Leiter, H. J., and Scortecci, F., "In Situ Thermal Characterization of the Accelerator Grid of an Ion Thruster," *Journal of Propulsion and Power*, Vol. 27, No. 3, 2011, pp. 532–537. https://doi.org/10.2514/1.50049

[18] Andreussi, T., Pieri, L., Albertoni, R., and Andrenucci, M., "Telemicroscopy Erosion Measurements of 5 kW-Class Hall Effect Thruster Channel Walls IEPC-2015-348 / ISTS-2015-b-348," 2015.

[19] Wirz, R. E., "Electrospray Thruster Performance and Lifetime Investigation for the LISA Mission," *AIAA Propulsion and Energy 2019 Forum*, American Institute of Aeronautics and Astronautics, 2019. https://doi.org/10.2514/6.2019-3816

[20] Basak, D., Noushkam, N., Glogowski, M., Crofton, M. W., and Young, J. A., "Sputtering Effects of Xenon Ion Thruster Plume on Common Spacecraft Materials," *AIAA SPACE 2015 Conference and Exposition*, American Institute of Aeronautics and Astronautics, 2015. https://doi.org/10.2514/6.2015-4642

[21] Celik, M., Batishchev, O., and Martinez-Sanchez, M., "Use of Emission Spectroscopy for Real-Time Assessment of Relative Wall Erosion Rate of BHT-200 Hall Thruster for Various Regimes of Operation," *Vacuum*, Vol. 84, No. 9, 2010, pp. 1085–1091. https://doi.org/10.1016/j.vacuum.2010.01.031

[22] King, L. B., "Transport-Property and Mass Spectral Measurements in the Plasma Exhaust Plume of a Hall-Effect Space Propulsion System," Ph.D. University of Michigan, United States -- Michigan.

[23] Duan, X., Guo, D., Cheng, M., Yang, X., and Guo, N., "Measurements of Channel Erosion of Hall Thrusters by Laser-Induced Fluorescence," *Journal of Applied Physics*, Vol. 128, No. 18, 2020, p. 183301. https://doi.org/10.1063/5.0020074

[24] Lee, B. C., Huang, W., Tao, L., Yamamoto, N., Gallimore, A. D., and Yalin, A. P., "A Cavity Ring-down Spectroscopy Sensor for Real-Time Hall Thruster Erosion Measurements," *Review of Scientific Instruments*, Vol. 85, No. 5, 2014, p. 053111. https://doi.org/10.1063/1.4879135

[25] Bundesmann, C., Eichhorn, C., Neumann, H., Scholze, F., Spemann, D., Tartz, M., Leiter, H. J., Gnizdor, R. Y., and Scortecci, F., "In Situ Erosion Measurement Tools for Electric Propulsion Thrusters: Triangular Laser Head and Telemicroscope," *EPJ Techniques and Instrumentation*, Vol. 9, No. 1, 2022, pp. 1–23. https://doi.org/10.1140/epjti/s40485-022-00076-z

[26] Ottaviano, A., Thuppul, A., Hayes, J., Dodson, C., Li, G. Z., Chen, Z., and Wirz, R. E., "*In Situ* Microscopy for Plasma Erosion of Complex Surfaces," *Review of Scientific Instruments*, Vol. 92, No. 7, 2021, p. 073701. https://doi.org/10.1063/5.0043002

[27] Nayar, S. K., and Nakagawa, Y., "Shape from Focus," *IEEE Transactions on Pattern Analysis and Machine Intelligence*, Vol. 16, No. 8, 1994, pp. 824–831. https://doi.org/10.1109/34.308479

[28] Billiot, B., Cointault, F., Journaux, L., Simon, J.-C., and Gouton, P., "3D Image Acquisition System Based on Shape from Focus Technique," *Sensors*, Vol. 13, No. 4, 2013, pp. 5040–5053. https://doi.org/10.3390/s130405040

[29] Zidar, D. G., and Rovey, J. L., "Hall-Effect Thruster Channel Surface Properties Investigation," *Journal of Propulsion and Power*, Vol. 28, No. 2, 2012, pp. 334–343. https://doi.org/10.2514/1.B34312

[30] Ziegler, J. F., and Biersack, J. P., "The Stopping and Range of Ions in Matter," *Treatise on Heavy-Ion Science: Volume 6: Astrophysics, Chemistry, and Condensed Matter*, edited by D. A. Bromley, Springer US, Boston, MA, 1985, pp. 93–129. https://doi.org/10.1007/978-1-4615-8103-1_3
[31] Yamamura, Y., and Shindo, S., "An Empirical Formula for Angular Dependence of Sputtering Yields," *Radiation Effects*, Vol. 80, Nos. 1–2, 1984, pp. 57–72. https://doi.org/10.1080/00337578408222489
[32] Meng Chen, Rohrbach, C., Neuffer, A., Barth, K.-L., and Lunk, A., "Simulation of Boron Nitride Sputtering Process and Its Comparison with Experimental Data," *IEEE Transactions on Plasma Science*, Vol. 26, No. 6, 1998, pp. 1713–1717. https://doi.org/10.1109/27.747890
[33] Smirnov, A., Raitses, Y., and Fisch, N. J., "Plasma Measurements in a 100 W Cylindrical Hall Thruster," *Journal of Applied Physics*, Vol. 95, No. 5, 2004, pp. 2283–2292. https://doi.org/10.1063/1.1642734
[34] Raitses, Y., Staack, D., Dunaevsky, A., Dorf, L., and Fisch, N., "Measurements of Plasma Flow in a 2 kW Segmented Electrode Hall Thruster," presented at the the 28th International Electric Propulsion Conference, Toulouse, France, 2003.